Nanoscale

PAPER

View Article Online
View Journal | View Issue

Cite this: *Nanoscale*, 2018, **10**, 1015

Catalytic synthesis of few-layer graphene on titania nanowires†

Akira Kudo, ‡[a] Sung Mi Jung,*§[b] Michael S. Strano,[c] Jing Kong[b] and Brian L. Wardle[d]

Received 8th August 2017,
Accepted 20th November 2017

DOI: 10.1039/c7nr05853e

rsc.li/nanoscale

Growth mechanisms of graphitic nanostructures on metal oxides by chemical vapor deposition (CVD) are observed at 750 °C, using titania nanowire aerogel (NWAG) as a three-dimensional substrate and without metal catalysts. We temporally observed catalytic transformation of amorphous carbon into few-layer graphene on the surface of 5–10 nm diameter titania nanowires. The graphitization spontaneously terminates when the titania nanowires are encapsulated by a shell of approximately three graphene layers. Extended CVD time beyond the termination point (>1125 seconds) yields only additional amorphous carbon deposits on top of the few-layer graphene. Furthermore, it was discovered that the islands of amorphous carbon do not graphitize unless they catalytically grow beyond a threshold size of 5–7 nm along the nanowire length, even after an extended thermal treatment. The electrical conductivity of the NWAG increased by four orders of magnitude, indicating that the graphene shell mediated by titania nanowires yielded a network of graphene throughout the three-dimensional nanostructure of the aerogel. Our results help us understand the growth mechanisms of few-layer graphene on nanostructured metal oxides, and inspire facile and controllable processing of metal oxide–nanocarbon fiber–shell composites.

Introduction

Carbon nanomaterials, such as carbon nanotubes (CNTs), carbon nanofibers (CNFs), and graphene, have been extensively researched for their prospective applications in electronics,[1,2] solar cells,[3,4] fuel cells,[5,6] and high performance composite materials.[7,8] Controlled synthesis of these nanostructures has also been developed by chemical vapor deposition (CVD), and the kinetics that govern the processes have been investigated.[9] While most CVD syntheses employ metal catalysts such as Fe nanoparticles or Cu sheets, metal oxides that are neither reduced to metal nor carbide during the CVD process have garnered researchers' attention, as both nanoparticle catalysts and substrates on which carbon nanomaterials are synthesized directly. Development of these new catalysts will not only lead to solutions for issues that prohibit full-fledged realization of potential applications of carbon nanomaterials,[10–13] but also elucidate the growth mechanisms of carbon nanomaterials with/on metal oxides.

Since the late 2000s, several metal oxide nanoparticles have been studied as non-metallic nanoparticle catalysts in order to synthesize CNTs, CNFs, and graphenes.[14–19] Accordingly, for these new nanoparticle catalysts, surface bound mechanisms of CNT/CNF growth that are different from those for metal nanoparticle catalysts are discussed.[20–22] Their low growth yield, however, has rendered the imaging of the interface between CNTs/CNFs and catalysts very difficult by high resolution transmission electron microscopy (HRTEM), leaving the mechanisms of graphitization unclear. Graphene sheets directly synthesized on non-metallic substrates by CVD are believed to nucleate from the surface defect sites such as steps or dislocations,[23,24] as proposed for metallic substrates.[25,26] Due to the two-dimensional nature of the graphene sheet, probing techniques are powerful tools to experimentally clarify these growth mechanisms at an atomic scale, especially scanning tunneling microscopy (STM) performed during the growth on electrically conductive substrates. For example, on a platinum substrate, nucleation of graphene was preferentially observed from steps rather than the middle of terraces.[27] On a

[a]*Department of Materials Science and Engineering, Massachusetts Institute of Technology, Cambridge, Massachusetts 02139, USA*
[b]*Department of Electrical Engineering and Computer Science, Massachusetts Institute of Technology, Cambridge, Massachusetts 02139, USA.*
E-mail: sungmijung@gmail.com; Tel: +1-617-324-4235
[c]*Department of Chemical Engineering, Massachusetts Institute of Technology, Cambridge, Massachusetts 02139, USA*
[d]*Department of Aeronautics and Astronautics, Massachusetts Institute of Technology, Cambridge, Massachusetts 02139, USA*

†Electronic supplementary information (ESI) available. See DOI: 10.1039/c7nr05853e

‡Current affiliation: California Institute of Technology, Pasadena, California, 91125, USA.
§Current affiliation: Future Environmental Research Center, Korea Institute of Toxicology, Jinju, 52834, Republic of Korea.

copper substrate, several types of nascent carbon clusters as intermediate states of graphene synthesis were resolved at the sub-nanometer scale during CVD by *in situ* STM.[28,29] However, STM is not viable if the substrate is not electrically conductive. Furthermore, visually acquiring atomic-scale information of the graphene–metal oxide interface is difficult with probing of a two-dimensional system, although highly desired for further understanding on growth mechanisms.

Here, we report the mechanisms of the catalytic synthesis of few-layer graphene on titania nanowire aerogel (NWAG). Using an *ex situ* aberration-corrected transmission electron microscope (Cs-corrected TEM), the process is tracked at an atomic scale from deposition and growth of amorphous carbon, and graphitization, to the formation of a graphitic shell that continuously encapsulates the surface of entangled titania nanowires. By investigating titania NWAG after CVD every 225 s up to 1575 s, we observe the termination of graphitization when the nanowire surface is uniformly covered by 2–3 layers of graphene at 1125 s. Longer CVD durations only result in an amorphous carbon layer on top of the previously synthesized graphene layers underneath, providing no distinct changes in the morphology. From these observations, we conclude that the graphitization is facilitated by the titania nanowire that serves as a nucleation surface as well as a catalyst. We also show that catalytic graphitization does not progress when maintaining the sample at an elevated temperature, but begins once the amorphous carbon grows beyond a certain threshold of the diameter. The effect of few-layer graphene on the titania NWAGs is highlighted by the increase in electrical conductivity by 4 orders of magnitude, consistent with the percolation theory. The value is comparable to the electrical conductivity of some full-carbon foams, proving that the titania nanowires formed a network of few-layer graphene, despite their lower catalytic activity than that of metal catalysts toward graphitization. Combining Cs-corrected TEM investigation and Raman spectroscopy, we find that the few-layer graphene shell encapsulates the nanowire surface continuously throughout the three-dimensionally entangled titania nanowires. This work provides insights into the mechanisms of metal catalyst-free graphitization on metal oxides whose structure is not limited to nanoparticles or flat substrates investigated so far.

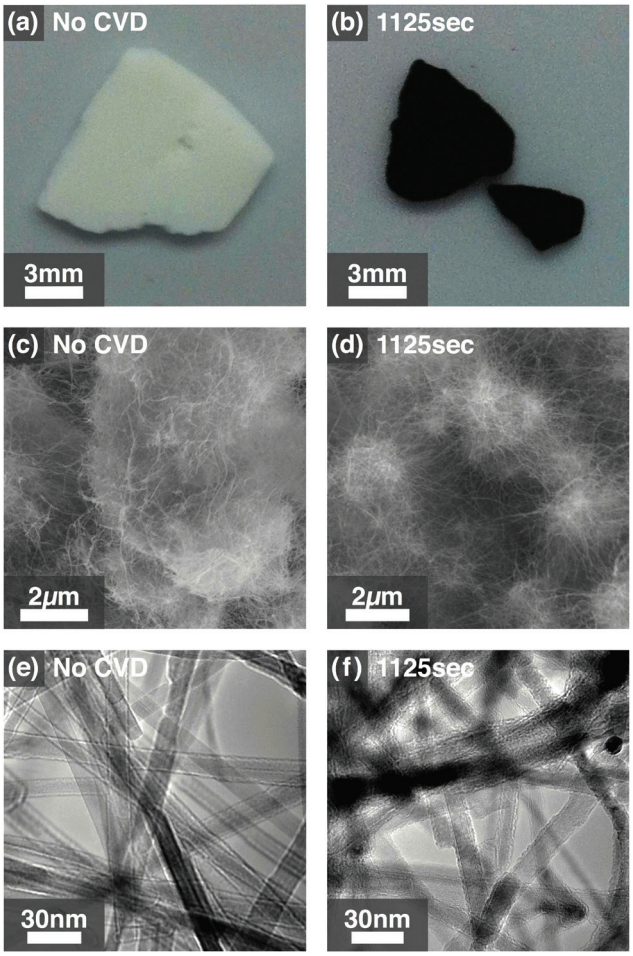

Fig. 1 Titania NWAG without CVD (left) and after 1125 s of CVD (right). The first line shows optical images of titania NWAG (a) without CVD and (b) after 1125 s CVD (not an identical piece of sample). A clear change in color is permanently observed. The second line shows SEM images of titania NWAG (c) without CVD and (d) after 1125 s CVD. The morphologies of two titania NWAG samples under SEM are almost identical. The third line shows TEM images of titania NWAG (e) without CVD and (f) after 1125 s CVD. Continuous deposition of carbon on each nanowire is observed after CVD.

Results and discussion

Fig. 1 juxtaposes titania NWAG samples before and after the CVD synthesis of graphitic layers (1125 s CVD) at different magnifications. The CVD parameters in this work are based on our previous work regarding the synthesis of graphitic carbon nanostructures with metal oxide nanoparticle catalysts, particularly titania metal oxide nanoparticle mediated CNT growth mechanisms[30] utilizing ethylene as a carbon feedstock. After ramping up the temperature to 750 °C under a flow of 100 sccm argon and 400 sccm hydrogen, the titania nanowire aerogel turns from white to black in the tube furnace before introducing ethylene. In a supplementary experiment, when taken out of the tube furnace at this stage, the NWAG aerogel changes from black to dark blue in a few minutes at room temperature and under atmospheric pressure. Thus, the pre-growth ramp at an elevated temperature reduced the titania nanowires into substoichiometric titanium oxide, and then in air the substoichiometric titanium oxide is partially re-oxidized.[31] Tsuyumoto *et al.* obtained dark blue substoichiometric titanium oxide by reducing reagent grade titania at 950 °C for 1 h under pure hydrogen, which is a more extreme reducing environment than we employed.[32] Chen *et al.* synthesized permanently black titanium oxide (TiO) nanoparticles after reduction at 200 °C for 5 days under a 20 bar hydrogen atmosphere.[33] Thus, the conditions used for the CVD growth of graphene on titania NWAG were not sufficient to reduce to metallic titanium, nor even to TiO, and therefore graphene

growth occurred on moderately reduced titania. After the CVD growth process for 1125 s, the aerogel remains black and does not return to the dark blue color when exposed to air, due to the deposition of carbon on the nanowires (Fig. 1a and b). The CVD gas flow infiltrates well into the bulk of these entangled nanowires, evidenced by the deposition of carbon that changed color not only on the surface of bulk titania NWAG but also in the interior of the millimeter-scale NWAG sample. We note that the titania NWAG shrinks by ~10% in each dimension after CVD, but the nanowires do not aggregate during CVD (Fig. 1c and d). Fig. 1e and f show carbon layers grown on nanowires after CVD, while the diameters of these nanowires remained unchanged. From these SEM and TEM images, the morphology of NWAG is observed to remain almost the same before and after the CVD, indicating that the high porosity of the titania NWAG is preserved.[34]

Fig. 2 compares the representative microscopic morphologies of the carbon deposit on the titania nanowire surface when imaged by Cs-corrected TEM, after CVD for different lengths of time up to 1125 s. In Fig. 2a, 0 s means that the temperature is elevated to 750 °C (with argon and hydrogen) and cooled down immediately without introducing ethylene. The nanowire surface after 0 s CVD shows surface defects but retains crystallinity at the nanowire surface after reduction. In Fig. 2b after 225 s of CVD, islands of amorphous carbon are formed with lengths less than 5 nm along the wire. Those amorphous carbons grow up to 675 s, while graphitization concurrently initiates around 675 s (Fig. 2c and d). The 900 s CVD shows some remaining amorphous carbon, seen as tiny clusters in Fig. 2e, but by 1125 s these are nearly completely incorporated into the graphitic nanostructures (Fig. 2f). The graphitic nanostructures after 1125 s have around three graphene layers.

1350 s or longer CVD does not grow additional graphitic layers apparently compared to the 1125 s CVD case; instead, we occasionally see an amorphous carbon layer on top of the graphitic nanostructures previously synthesized (Fig. 3a and b). The nanowire surface is covered with graphitic layers and an additional amorphous carbon layer, on the outer surface as indicated by yellow arrows. The electron diffraction pattern was taken at a lower magnification (Fig. S1†). It does not show clear diffraction patterns indicative of a graphitic structure, implying that the graphitic layers are defect-rich and not highly crystalline. The two-layer structure of amorphous carbon on few-layer graphene is also seen after 1575 s CVD. The amorphous carbon is clearly different from the soot observed on titania NWAG after 900 s CVD at 850 °C, where we see the onset of severe gas-phase pyrolysis of ethylene (see Fig. S2†). Approximately 7 nanometer-thick carbon soot is deposited coaxially around the titania nanowire surface after 900 s of CVD. The soot shows traces of graphitic layers by HRTEM and hence is not an amorphous structure, presumably because pyrolysis at 850 °C in the 1 inch quartz tube converts ethylene into nano-graphene sheets in the gas phase. According to these morphologies, amorphous carbons at 750 °C are graphitized *via* the titania nanowire surfaces. The graphitization is terminated once the graphitic nanostructures cover all the titania nanowire surfaces, further evidencing the catalytic activity of titania nanowires toward graphitization *via* CVD. The sample after 1350 s CVD is investigated by X-ray

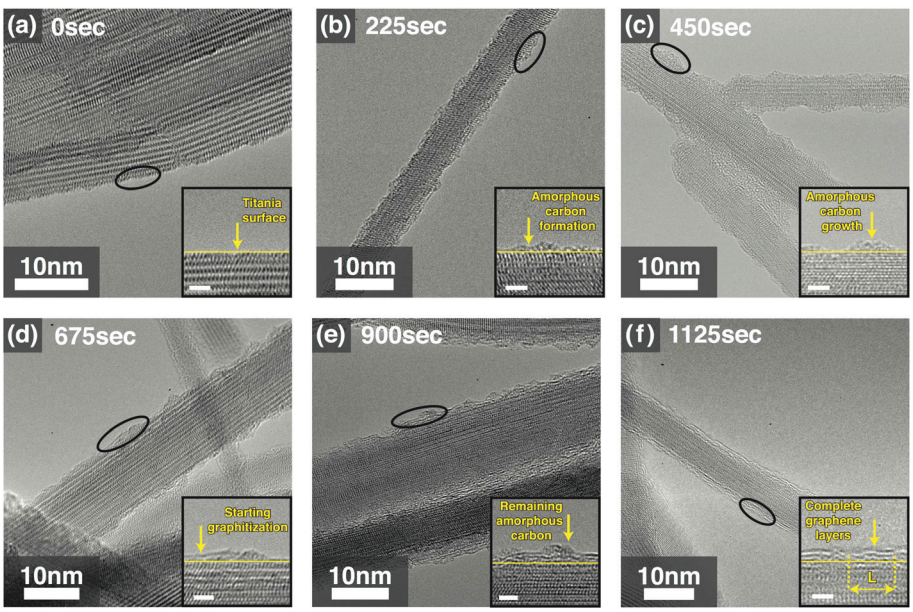

Fig. 2 Temporal study of NWAG after CVD graphene processing for (a) 0 s, (b) 225 s, (c) 450 s, (d) 675 s, (e) 900 s, and (f) 1125 s. Insets magnify the area indicated by black ellipsoids, featuring the representative carbon morphology at each time step by yellow arrows. Yellow lines in insets indicate the boundary between the carbon deposit and the nanowire surface. Scale bars in insets are 2 nm. The inset of (f) also annotates the definition of measured graphitic domain size *L* along the nanowire length.

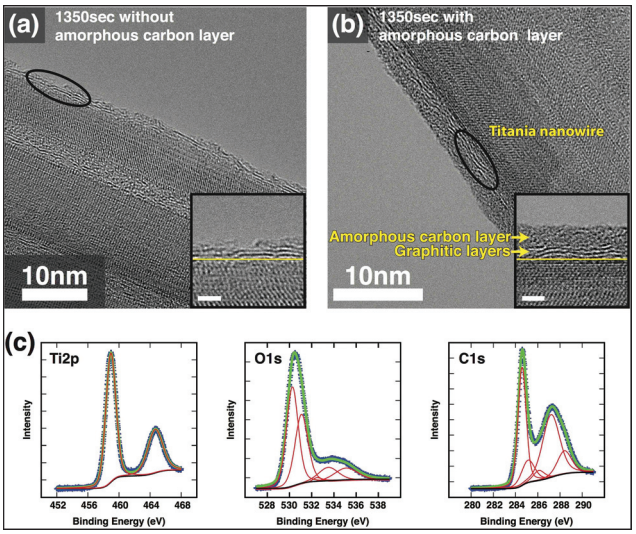

Fig. 3 Study of NWAG after CVD for 1350 s. (a) A HRTEM image of an area without amorphous carbon shows an approximately 3 layer-thick graphitic structure similar to the sample after 1125 s CVD, indicating no further graphitic layer. (b) A HRTEM image of another area shows that an amorphous carbon layer starts being deposited over graphitic layers as noted. (C) XPS spectra of titanium, oxygen, and carbon. Blue plots are raw data, black curves are Shirley background, red curves are fitting curves for each component, and green curves are the sum of fitting curves.

photoelectron spectroscopy (XPS) to study the chemical state of the titania nanowires and CVD-grown carbon layers (Fig. 3c). After subtracting the Shirley background, the obtained spectra were separated and fitted to a pseudo-Voigt function which is a linear combination of weighted Gaussian and Lorentzian functions with the Gaussian fraction being 70–80%.[35,36] The spectrum of titanium (Ti 2p) is obtained from Ti^{4+} (459.0 eV for Ti $2p_{3/2}$ and 464.7 eV for Ti $2p_{1/2}$),[37] showing no major peaks from titanium carbide,[37] titanium metal,[38] nor reduced titanium oxide (Ti_2O_3 and TiO).[38] This is consistent with the discussion regarding the lack of reduction of titania nanoparticles in our similar prior CVD work.[30] The spectrum of oxygen (O 1s) is separated into 5 components: lattice oxygen in TiO_2 (530.3 eV),[39] carbonyl group on aromatic carbon (531.1 eV),[35,39] C–O bonding with aliphatic carbon (532.5 eV),[35] C–O bonding with aromatic carbon (533.5 eV),[35,39] and chemisorbed water (535.1 eV).[40] The spectrum of carbon (C 1s) is also separated into 5 components: sp^2 hybridized carbon (284.6 eV),[40,41] sp^3 hybridized carbon (285.1 eV),[40,41] C–O bonding (286.1 eV),[35] carbonyl group (287.2 eV),[35] and carboxyl group (288.4 eV).[35] C–O bonding includes hydroxyl and epoxy groups that can be found on the basal plane of graphene sheets.[42,43] A peak from titanium carbide is absent in this C 1s spectrum too.[44] As observed in O 1s and C 1s spectra, the peak of the carbonyl group has the highest intensity among those from expected functional groups, indicating that the deposited carbon depleted oxygen from titania nanowires and is oxidized especially on the edge sites of the graphitic layers rather than on the basal plane.[42,43]

In order to track the catalytic graphitization more quantitatively, Raman spectra are taken from all the samples with an excitation wavelength of 532 nm (Fig. 4a). According to Ferrari *et al.*,[45] the Raman spectra between 1000 and 1800 cm^{-1} are separated into 5 peaks corresponding to the sp3 component (1200 cm^{-1}), D peak (1340 cm^{-1}), amorphous carbon (1510 cm^{-1}), G peak (1590 cm^{-1}), and D′ peak (1620 cm^{-1}). Raman shifts for each separated peak are approximate, based on the literature.[46,47] The peak corresponding to the amorphous carbon component is fitted to the Gaussian function, while others are fitted to the Lorentzian function. See Fig. S3† for the fitting procedure and examples of Raman spectra separated into the components. The D and G peaks are more clearly separated as the reaction time extends, indicating that the amount of amorphous carbon relative to graphitic carbon reduces. Peak area ratios are plotted in Fig. 4(b) for D peak *vs.*

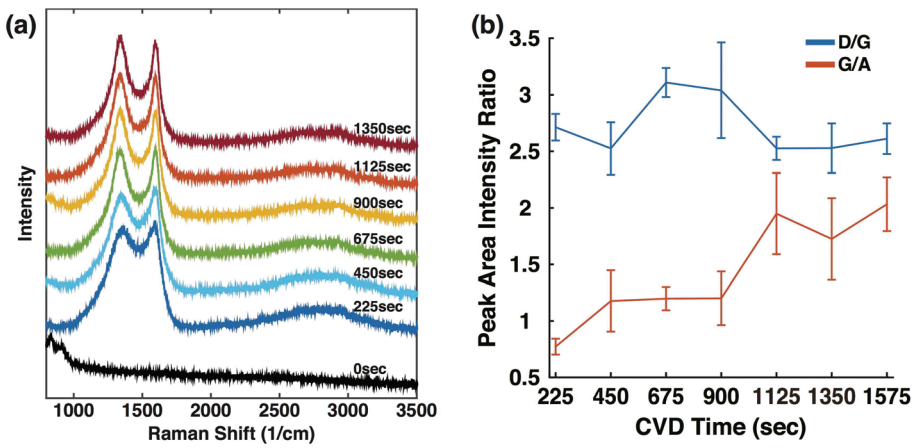

Fig. 4 Raman spectra analysis. (a) Raman spectra from NWAG and graphene-encapsulated NWAG after CVD for different time lengths. D and G peaks are clearly divided as the CVD time extends. A broad peak around 2800 cm^{-1} is also gradually separated into two major components for longer CVD times: 2D and D + D′ peaks. (a) D/G and G/A peak area intensity ratios for the samples after CVD. The error bars indicate standard deviation.

G peak (D/G) and G peak *vs.* A peak (G/A). Samples after 225 and 450 s CVD have peaks at the D and G peaks which could be attributed to different origins[47] or occasional graphitization at intersections of titania nanowires as observed in Fig. 2c. At 675 s, the D/G ratio increases due to the initiation of graphitization, which forms tiny graphitic platelets that give rise to a high D peak intensity.[45] A broad peak around 2800 cm^{-1} separates into 2D peak (~2670 cm^{-1}) and D + D′ (~2980 cm^{-1}) peak after 675 s CVD, also indicating the formation of graphene layers.[48,49] Between 900 and 1125 s, two radical changes are observed: the D/G ratio reduces and the G/A ratio increases. Thereafter both intensity ratios level off. As shown in Fig. 2e and f, most of the amorphous carbon was converted into graphitic nanostructures which ceased at 1125 s CVD. The increase in the G/A ratio is attributed to the graphitization of the remaining amorphous carbon, and the decrease in the D/G ratio is due to the increase in the number of graphitic layers[50] rather than the improved crystallinity of the graphitic nanostructures which will be discussed later.

Furthermore, isothermal annealing was implemented in order to investigate its effect on the structure of amorphous carbon. Samples after 450 s CVD were followed by another 450 and 900 s isothermal annealing under an argon flow, *i.e.*, the H_2 and ethylene flow ceased at 450 s. In Fig. 5, these samples are compared with the sample just after 450 s CVD by Raman spectroscopy. No clear evidence is observed for improved graphitization after annealing. As seen in Fig. 2c, the islands of amorphous carbon are separated from each other after 450 s CVD. The results of isothermal annealing explain that the amorphous carbons were not graphitized by annealing. Considering the nanometer-scale dimensions of the islands of amorphous carbon, it seems that the higher surface energy of graphite[51] when compared to that of amorphous carbon[52] prevented graphitization; although, thermodynamically graphite is preferred to amorphous carbon.[53]

Graphitization would occur after the amorphous carbons reach a "threshold" by growing larger. A single island of amorphous carbon may solely grow to reach the threshold size, or two or more islands may merge as each of them grows. The threshold size can be obtained from two processes by analyzing the graphitic domain size L, the approximate diameter of the single crystal of few-layer graphene. First, we estimate the size from the Raman spectra using a formula that relates the mean diameter of the graphite domain, corresponding to L, to the full width at half maximum (FWHM) of a G peak.[54] According to the analysis, L increases monotonically as the CVD time increases and eventually levels off at 900 s. We also measure the size of single graphitic domain along the nanowire length from HRTEM images as representative of L at each CVD time (annotated in the inset of Fig. 2(f)). The results of estimation and measurement are plotted in Fig. 6, providing the same trend as estimated from the formula but generally smaller than that by about 2 nm. L is estimated to be 5–7 nm along the nanowire length at 675 s CVD where graphitization initiates. Therefore, the threshold size for the islands of amorphous carbon to graphitize is expected to be similar to this value. Ls levels off after 900 s around 6–8.5 nm, indicating that the curvature of the nanowire may hinder further growth of the graphitic domain.

The bulk electrical conductivity of titania NWAG as a function of different CVD times is investigated as shown in Fig. 7. An increase in electrical conductivity by four orders of magnitude is observed after 675 s CVD, explained by the percolation of electrically conductive paths by few-layer nanographene. Electrical conductivity mostly levels off at 900 s after a slight increase between 675 and 900 s, corresponding to the completion of the conductive path associated with further graphitization. The electrical conductivity after 1125 s CVD is 2.42 S m^{-1}, comparable to some full-carbon foams previously reported,[55,56] which indicates that the synthesized few-layer graphene patches are networked through the titania MWAG. The electrical conductivity can be improved by modifying the process that controls the number density of titania nanowires per nominal volume, since the morphology of NWAG is preserved after CVD.

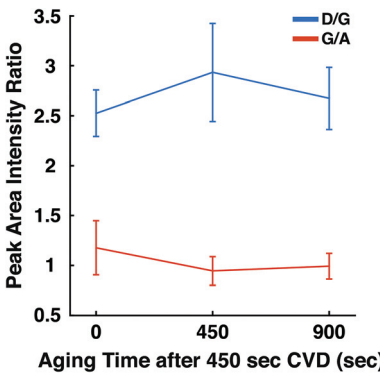

Fig. 5 D/G and G/A ratios of samples after different aging time lengths following 450 s CVD. The error bars indicate standard deviation.

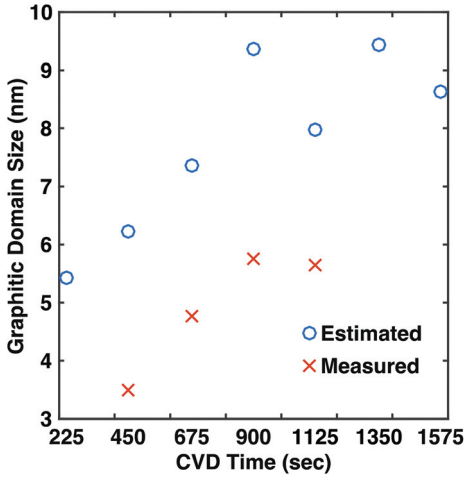

Fig. 6 Graphitic domain size L for each CVD time length obtained from estimation by the formula and measurement of the single domain size from HRTEM images. Both processes yielded the same trend that the L levels off at 900 s CVD.

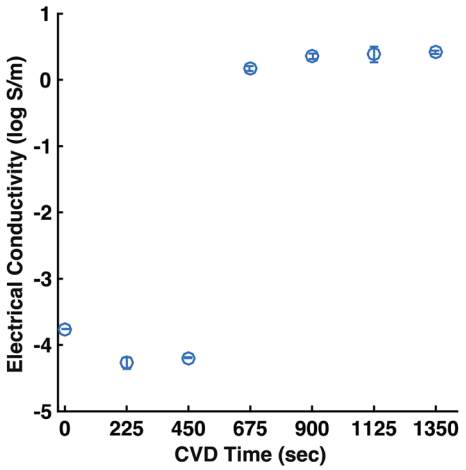

Fig. 7 Electrical conductivity of titania NWAG after graphene synthesis as a function of growth time. The error bars indicate standard deviation.

Combining the electrical conductivity measurement, HRTEM investigation, Raman spectra, and the estimation on the mean domain size L, the mechanisms of graphitic nanostructure growth are summarized as follows: (1) amorphous carbons grow until they attain the minimum size to be graphitized around 675 s, causing a jump in the G/D ratio. The graphitic nanostructures start to connect with each other to build a conductive path and increase the electrical conductivity of the NWAG. Then, (2) graphitization proceeds through 900 s when the electrical conductivity levels off, while amorphous carbon remains on its exterior as in Fig. 2e. Next, (3) at around 1125 s, the number of graphene layers increase to a maximum (the D/G ratio decreases and levels off thereafter), and the remaining amorphous carbon is converted almost completely (the jump in the G/A ratio). Finally (4) for CVD longer than 1125 s, an amorphous carbon layer may occasionally be formed on top of the graphitic nanostructure as seen in Fig. 3 because catalytically active surfaces of titania nanowires are inaccessible for adsorbed feedstock molecules. Our observations and analysis suggest that titania nanowire surfaces serve as catalysts to facilitate graphitization which would only be realized at much higher temperatures without catalysts.[57] Among the published work regarding graphitization on metal oxides, a similar result is reported using magnesia nanoparticles by Rümmeli *et al.*[19] which shows that the number of graphene layers did not change as a function of CVD time. The graphitic nanostructures synthesized in this work are thinner and more homogeneous than those grown on magnesia nanoparticles.

Conclusion

In conclusion, the CVD growth of graphitic nanostructures on titania NWAGs is studied at 750 °C using ethylene. The catalytic conversion of amorphous carbon to few-layer nanographene is characterized using Cs-corrected TEM micrographs for different CVD times. Graphitization typically terminates when the structures are about 3 layer-thick, indicating that the titania nanowire surface facilitates graphitization to few-layer graphene. Analysis of the graphitic domain size indicates that an island of amorphous carbon has to grow beyond the threshold size of 6–8.5 nm in diameter to be catalytically graphitized. The graphitic layers form a continuous network throughout the intricate three-dimensional structure of the titania NWAG, improving the electrical conductivity from a standard value for titania to a value comparable to those of some all-carbon foams, while retaining the porosity of the titania NWAG. As the graphene-on-titania heterostructure has likely direct applications in energy[58,59] and electrochemical technologies,[60] studying its performance in these applications is recommended as future work. The results herein potentially apply more broadly to the mechanisms of graphitic nanostructure formation on metal oxides with a variety of species and shapes.

Methods

Synthesis of TiO_2 nanowire aerogel

Commercially available anatase TiO_2 nanoparticles (Aeroxide@ TiO_2 P25, Evonik Industries) were dissolved in 10 M KOH at the ratio of 7.5 mg ml^{-1}. The mixture was stirred for 30 min and transferred to a Teflon vessel held in a stainless steel vessel. The sealed vessels were placed in a furnace and kept at 453 K for 8 h–16 h. During hydrothermal synthesis, $K_2Ti_8O_{17}$ nanowires were grown and physically interlinked to each other to form $K_2Ti_8O_{17}$ nanowire hydrogel. The $K_2Ti_8O_{17}$ nanowire hydrogel was ion-exchanged into $H_2Ti_8O_{17}$ by acid treatment (0.2 M HNO_3). The $H_2Ti_8O_{17}$ nanowire hydrogel was then washed with excess DI water by repeatedly soaking and replacing the water until pH 5.5–6 of the supernatant was reached. The hydrogels were then cut into various shapes with a blade and subsequently placed into anhydrous ethanol overnight for solvent exchange. After that, the $H_2Ti_8O_{17}$ nanowire hydrogels were dried into aerogels by using a critical point drier. Finally, $H_2Ti_8O_{17}$ NWAGs were converted into anatase TiO_2 NWAGs by heating at 600 °C for 2 h in air using fused quartz process tubes (25 mm OD × 22 mm ID × 76.2 cm length) placed inside a Lindberg/Blue M MiniMite 1 inch diameter electric clamshell tube furnace. The process tubes used in this work were baked in air at 800 °C for 1 h to eliminate potential contamination if needed.

Synthesis of graphitic layers on TiO_2 nanowire aerogel

Argon, hydrogen, and ethylene (Airgas, UHP grade, 99.999%) were used for CVD. All the CVD in this work was performed under atmospheric pressure. NWAG samples were first inserted into the quartz CVD tube. Then, the process tube was flushed with 750 sccm of argon at room temperature for 2 min to remove residual air from the tube. Next, a flow of 400 sccm of hydrogen and 100 sccm of argon was introduced and the temperature was ramped to 750 °C at ~55 °C min^{-1}. Once at

the set point, a flow of 200 sccm of ethylene was added, and the flow rate of hydrogen was reduced to 300 sccm. After each CVD time length (0, 225, 450, 675, 900, 1125, 1350, 1575 s), the hydrogen and ethylene were turned off and the system was cooled to room temperature. For isothermal annealing, hydrogen and ethylene flows were ceased after 450 s CVD and the sample was kept under a flow of 600 sccm argon at 750 °C for another 450 and 900 s. After that, the system was cooled to room temperature.

Characterization

Cs-corrected TEM (Zeiss Libra 80-200) was used to characterize the resulting morphology of carbon deposition and investigate the transformation mechanism of amorphous carbon into graphitic nanostructures. Raman spectroscopy (Horiba Jobin Yvon HR 800 and Renishaw M1000 Micro Raman Spectrometer System) was used to quantitatively analyze the evolution of graphitization. Manual fitting for the obtained spectra into individual components is done by a program coded in C, and the accuracy of the fitting is evaluated by normal probability plots. The electrical conductivity was measured using a 4 point probe (Keithley SCS-4200). The depth of the electrode into NWAG samples was 0.5 mm, and the NWAG samples were not compressed. XPS spectra were corrected using a Shimadzu Kratos Axis NOVA with an approximate spot size of 0.8 mm^2. The same program and manual fitting procedure as used for Raman spectra were applied to analyze the XPS spectra.

Conflicts of interest

There are no conflicts to declare.

Acknowledgements

This material is based upon the work supported by the National Science Foundation under Grant No. 1007793 and was also supported by Airbus Group, Embraer, Lockheed Martin, Saab AB, ANSYS, Hexcel, and TohoTenax through MIT's Nano-Engineered Composite aerospace STructures (NECST) Consortium. This work made use of the Shared Experimental Facilities supported in part by the MRSEC Program of the National Science Foundation under award number DMR-0819762 and the facilities at the MIT Institute for Soldier Nanotechnologies (ISN), supported by the U.S. Army Research Office under contract W911NF-13-D-0001. This work was performed in part at the Center for Nanoscale Systems (CNS), a member of the National Nanotechnology Infrastructure Network (NNIN), which is supported by the National Science Foundation under NSF award no. ECS-0335765. CNS is part of Harvard University. This research was also supported by the Individual Basic Science&Engineering Research Program through the National Research Foundation of Korea (NRF) funded by the Ministry of Science, ICT & Future Planning (NRF-2017R1D1A1B03033694). A. Kudo also thanks Dr Kehang Cui (MIT) for the discussion regarding Raman spectrum data, Prof. George R. Rossman (Caltech) for providing access to a Renishaw M1000 Micro Raman Spectrometer System, and Pakpoom Buabthong (Caltech) for collecting XPS data.

References

1 H. Wang, P. Wei, Y. Li, J. Han, H. R. Lee, B. D. Naab, N. Liu, C. Wang, E. Adijanto, B. C.-K. Tee, S. Morishita, Q. Li, Y. Gao, Y. Cui and Z. Bao, *Proc. Natl. Acad. Sci. U. S. A.*, 2014, **111**, 4776–4781.
2 A. Shimoni, S. Azoubel and S. Magdassi, *Nanoscale*, 2014, **6**, 11084–11089.
3 M. R. Golobostanfard, H. Abdizadeh and S. Mohajerzadeh, *Nanotechnology*, 2014, **25**, 345402.
4 Z. Wu, S. Bai, J. Xiang, Z. Yuan, Y. Yang, W. Cui, X. Gao, Z. Liu, Y. Jin and B. Sun, *Nanoscale*, 2014, **6**, 10505–10510.
5 F. Gao, G.-L. Zhao and S. Yang, *ACS Catal.*, 2014, **4**, 1267–1273.
6 A. Paneri, Y. Heo, G. Ehlert, A. Cottrill, H. Sodano, P. Pintauro and S. Moghaddam, *J. Membr. Sci.*, 2014, **467**, 217–225.
7 I. Y. Stein and B. L. Wardle, *Carbon*, 2014, **68**, 807–813.
8 V. Mittal, A. U. Chaudhry and G. E. Luckachan, *Mater. Chem. Phys.*, 2014, **147**, 319–332.
9 G. Eres, M. Regmi, C. M. Rouleau, J. Chen, I. N. Ivanov, A. A. Puretzky and D. B. Geohegan, *ACS Nano*, 2014, **8**, 5657–5669.
10 S. Boncel and K. K. K. Koziol, *Appl. Surf. Sci.*, 2014, **301**, 488–491.
11 A. Reina, H. Son, L. Jiao, B. Fan, M. S. Dresselhaus, Z. Liu and J. Kong, *J. Phys. Chem. C*, 2008, **112**, 17741–17744.
12 C. Ge, Y. Li, J.-J. Yin, Y. Liu, L. Wang, Y. Zhao and C. Chen, *NPG Asia Mater.*, 2012, **4**, e32.
13 H. H. Kim, Y. Chung, E. Lee, S. K. Lee and K. Cho, *Adv. Mater.*, 2014, **26**, 3213–3217.
14 S. A. Steiner, T. F. Baumann, B. C. Bayer, R. Blume, M. A. Worsley, W. J. MoberlyChan, E. L. Shaw, R. Schlögl, A. J. Hart, S. Hofmann and B. L. Wardle, *J. Am. Chem. Soc.*, 2009, **131**, 12144–12154.
15 B. Liu, D.-M. Tang, C. Sun, C. Liu, W. Ren, F. Li, W.-J. Yu, L.-C. Yin, L. Zhang, C. Jiang and H.-M. Cheng, *J. Am. Chem. Soc.*, 2011, **133**, 197–199.
16 Q. Cai, Y. Hu, Y. Liu and S. Huang, *Appl. Surf. Sci.*, 2012, **258**, 8019–8025.
17 B. C. Bayer, C. Castellarin-Cudia, R. Blume, S. A. Steiner, C. Ducati, D. Chu, A. Goldoni, A. Knop-Gericke, R. Schlögl, C. Cepek, J. Robertson and S. Hofmann, *RSC Adv.*, 2013, **3**, 4086–4092.
18 P. R. Kidambi, B. C. Bayer, R. S. Weatherup, R. Ochs, C. Ducati, D. V. Szabó and S. Hofmann, *Phys. Status Solidi RRL*, 2011, **5**, 341–343.
19 M. H. Rümmeli, A. Bachmatiuk, A. Scott, F. Börrnert, J. H. Warner, V. Hoffman, J.-H. Lin, G. Cuniberti and B. Büchner, *ACS Nano*, 2010, **4**, 4206–4210.

20 Y. Homma, H. Liu, D. Takagi and Y. Kobayashi, *Nano Res.*, 2009, **2**, 793.
21 A. Kudo, S. A. Steiner, B. C. Bayer, P. R. Kidambi, S. Hofmann, M. S. Strano and B. L. Wardle, *J. Am. Chem. Soc.*, 2014, **136**, 17808–17817.
22 A. J. Page, S. Saha, H.-B. Li, S. Irle and K. Morokuma, *J. Am. Chem. Soc.*, 2015, **137**, 9281–9288.
23 K. Saito and T. Ogino, *J. Phys. Chem. C*, 2014, **118**, 5523–5529.
24 S. Tang, G. Ding, X. Xie, J. Chen, C. Wang, X. Ding, F. Huang, W. Lu and M. Jiang, *Carbon*, 2012, **50**, 329–331.
25 S. Saadi, F. Abild-Pedersen, S. Helveg, J. Sehested, B. Hinnemann, C. C. Appel and J. K. Nørskov, *J. Phys. Chem. C*, 2010, **114**, 11221–11227.
26 J. Gao, J. Yip, J. Zhao, B. I. Yakobson and F. Ding, *J. Am. Chem. Soc.*, 2011, **133**, 5009–5015.
27 X. Feng, J. Wu, A. T. Bell and M. Salmeron, *J. Phys. Chem. C*, 2015, **119**, 7124–7129.
28 T. Niu, M. Zhou, J. Zhang, Y. Feng and W. Chen, *J. Am. Chem. Soc.*, 2013, **135**, 8409–8414.
29 J. Zhang, Z. Wang, T. Niu, S. Wang, Z. Li and W. Chen, *Sci. Rep.*, 2014, **4**, 4431.
30 A. Kudo, S. A. Steiner, B. C. Bayer, P. R. Kidambi, S. Hofmann, M. S. Strano and B. L. Wardle, *J. Appl. Phys.*, 2017, **122**, 14301.
31 E. Carter, A. F. Carley and D. M. Murphy, *J. Phys. Chem. C*, 2007, **111**, 10630–10638.
32 I. Tsuyumoto and H. Uchikawa, *J. Mater. Sci. Lett.*, 2000, **19**, 2075–2076.
33 X. Chen, L. Liu, P. Y. Yu and S. S. Mao, *Science*, 2011, **331**, 746–750.
34 S. M. Jung, H. Y. Jung, W. Fang, M. S. Dresselhaus and J. Kong, *Nano Lett.*, 2014, **14**, 1810–1817.
35 A. Ganguly, S. Sharma, P. Papakonstantinou and J. Hamilton, *J. Phys. Chem. C*, 2011, **115**, 17009–17019.
36 J.-Y. Ruzicka, F. Abu Bakar, C. Hoeck, R. Adnan, C. McNicoll, T. Kemmitt, B. C. Cowie, G. F. Metha, G. G. Andersson and V. B. Golovko, *J. Phys. Chem. C*, 2015, **119**, 24465–24474.
37 M. M. O. Thotiyl, S. A. Freunberger, Z. Peng, Y. Chen, Z. Liu and P. G. Bruce, *Nat. Mater.*, 2013, **12**, nmat3737.
38 I. Milošev, M. Metikoš-Huković and H.-H. Strehblow, *Biomaterials*, 2000, **21**, 2103–2113.
39 J. Zhong, F. Chen and J. Zhang, *J. Phys. Chem. C*, 2010, **114**, 933–939.
40 L. Stobinski, B. Lesiak, A. Malolepszy, M. Mazurkiewicz, B. Mierzwa, J. Zemek, P. Jiricek and I. Bieloshapka, *J. Electron Spectrosc. Relat. Phenom.*, 2014, **195**, 145–154.
41 J. Díaz, G. Paolicelli, S. Ferrer and F. Comin, *Phys. Rev. B: Condens. Matter Mater. Phys.*, 1996, **54**, 8064–8069.
42 Y. L. Zhong, Z. Tian, G. P. Simon and D. Li, *Mater. Today*, 2015, **18**, 73–78.
43 A. Y. Sheng Eng, C. Kiang Chua and M. Pumera, *Nanoscale*, 2015, **7**, 20256–20266.
44 J. Yu, G. Dai, Q. Xiang and M. Jaroniec, *J. Mater. Chem.*, 2011, **21**, 1049–1057.
45 A. C. Ferrari and J. Robertson, *Phys. Rev. B: Condens. Matter Mater. Phys.*, 2000, **61**, 14095–14107.
46 Y. Ohgi, A. Ishihara, K. Matsuzawa, S. Mitsushima, K. Ota, M. Matsumoto and H. Imai, *J. Electrochem. Soc.*, 2013, **160**, F162–F167.
47 J. Schwan, S. Ulrich, V. Batori, H. Ehrhardt and S. R. P. Silva, *J. Appl. Phys.*, 1996, **80**, 440–447.
48 M. S. Dresselhaus, A. Jorio, M. Hofmann, G. Dresselhaus and R. Saito, *Nano Lett.*, 2010, **10**, 751–758.
49 A. C. Ferrari and D. M. Basko, *Nat. Nanotechnol.*, 2013, **8**, 235–246.
50 A. Reina, X. Jia, J. Ho, D. Nezich, H. Son, V. Bulovic, M. S. Dresselhaus and J. Kong, *Nano Lett.*, 2009, **9**, 30–35.
51 H. Zaidi, F. Robert and D. Paulmier, *Thin Solid Films*, 1995, **264**, 46–51.
52 J. S. Chen, S. P. Lau, B. K. Tay, G. Y. Chen, Z. Sun, Y. Y. Tan, G. Tan and J. W. Chai, *J. Appl. Phys.*, 2001, **89**, 7814–7819.
53 R. C. Powles, N. A. Marks, D. W. M. Lau, D. G. McCulloch and D. R. McKenzie, *Carbon*, 2013, **63**, 416–422.
54 O. A. Maslova, M. R. Ammar, G. Guimbretière, J.-N. Rouzaud and P. Simon, *Phys. Rev. B: Condens. Matter Mater. Phys.*, 2012, **86**, 134205.
55 M. Mecklenburg, A. Schuchardt, Y. K. Mishra, S. Kaps, R. Adelung, A. Lotnyk, L. Kienle and K. Schulte, *Adv. Mater.*, 2012, **24**, 3486–3490.
56 Z. Yu, M. McInnis, J. Calderon, S. Seal, L. Zhai and J. Thomas, *Nano Energy*, 2015, **11**, 611–620.
57 R. E. Franklin, *Proc. R. Soc. London, Ser. A*, 1951, **209**, 196–218.
58 L. Jiang, X. Lu, C. Xie, G. Wan, H. Zhang and T. Youhong, *J. Phys. Chem. C*, 2015, **119**, 3903–3910.
59 J. Zhao, J. Wu, F. Yu, X. Zhang, Z. Lan and J. Lin, *Electrochim. Acta*, 2013, **96**, 110–116.
60 M. R. Hasan, S. B. A. Hamid and W. J. Basirun, *Appl. Surf. Sci.*, 2015, **339**, 22–27.

